

Research Paper



The Holocene 1\_9 © The Author(s) 2021 Article reuse guidelines: sagepub.com/iournals-permissions DOI: 10.1177/09596836211033218 journals.sagepub.com/home/hol



# Timing and structure of early-Holocene climate anomalies inferred from north Chinese stalagmite records

Wuhui Duan, 1,2,3 D Zhibang Ma, Ming Tan, Hai Cheng,4,5 R. Lawrence Edwards, <sup>6</sup> Xinyu Wen, <sup>7</sup> Xuefeng Wang<sup>1</sup> and Lisheng Wang

#### **Abstract**

In this paper, a new decadal resolution stalagmite  $\delta^{18}$ O record covering 10.4–6.5 ka BP from Kulishu cave in Beijing, north China is presented in combination with the published stalagmite  $\delta^{18}$ O record covering 10.4–14.0ka BP in the same cave. Five significant monsoon collapses were identified around 11.5, 11.0, 10.0, 9.4, and 8.2 ka BP as well as three smaller ones around 10.3, 9.0, and 8.6 ka BP. The weak monsoon episodes around 8.6 and 8.2 ka BP form the two-step structure of the 8.2 ka event. All monsoon collapses, coeval with the cooling in northern high-latitude records, are correlated with Lakes Agassiz-Ojibway outbursts. Thus, our data support the idea of freshwater forcing of abrupt climate anomalies during the early Holocene. Nevertheless, the decreased irradiance together with freshwater outburst may account for the 9.2/9.3 ka event, which is expressed more significantly in low-latitude records.

### **Keywords**

cave records, climate anomalies, early Holocene, North China, structure, timing

Received 12 May 2021; revised manuscript accepted 15 June 2021

### Introduction

Multiple lines of evidence indicate that the relative stability of the early Holocene climate was punctuated by a series of abrupt climate oscillations (Bond et al., 2001; Jennings et al., 2015; Rasmussen et al., 2007; Yang et al., 2019). The most prominent of these, at around 8.2 ka BP (the 8.2 ka event), has been substantiated to be a global climate anomaly (Alley et al., 1997; Came et al., 2007; Cheng et al., 2009). Several high-resolution records suggest a twostep structure of the 8.2 ka event, with a preceding cooling at around 8.5 ka BP and peak cooling at around 8.2 ka BP (Liu et al., 2013; Rohling and Pälike, 2005; Tan et al., 2020), which was normally linked to the two-step release of Lake Agassiz freshwater (Clarke et al., 2004; Jennings et al., 2015; Teller and Leverington, 2004). However, the timing and duration of other climate anomalies during the early Holocene remain unclear. For example, although the 9.2/9.3 ka event has also been widely recognized (Dykoski et al., 2005; Fleitmann et al., 2008; Rasmussen et al., 2007) and mainly ascribed to the freshwater outburst from Lake Superior (Porinchu et al., 2019; Young et al., 2011, 2013; Yu et al., 2010), the amplitude in different records varies geographically. This event is very significant and even stronger than the 8.2ka event in most low-latitude records (Dykoski et al., 2005; Fleitmann et al., 2008; Gupta et al., 2003; Zhang et al., 2018b) but very modest and even absent from most mid-high latitude records (Boch et al., 2009; Dong et al., 2018; Porinchu et al., 2019; Rasmussen et al., 2007; Tan et al., 2020; Yang et al., 2019). Accordingly, the low-latitude hydrological process provoked directly by solar activity was suggested to play an important role in this anomaly (Zhang et al., 2018b). However, the

9.2/9.3 ka event is well expressed in a few high-latitude records, such as Arolik lake and Ammersee lake records (Grafenstein et al., 1999; Hu et al., 2003). Thus, more data are needed to explore the spatial pattern of the 9.2/9.3 ka event. Additionally, the Preboreal

Oscillation (PBO) and other smaller anomalies are identified at around 11.4, 11.1, and 10.0 ka BP in NGRIP δ<sup>18</sup>O record and a few terrestrial records (Björck et al., 2001; Cai et al., 2008; Rasmussen et al., 2007), which were mainly ascribed to smaller Agassiz outbursts. However, because of the different age uncertainties and resolutions, the correlation among these records is very tenuous,

<sup>1</sup>Key Laboratory of Cenozoic Geology and Environment, Institute of Geology and Geophysics, Chinese Academy of Sciences, China <sup>2</sup>CAS Center for Excellence in Life and Paleoenvironment, China <sup>3</sup>Connected Waters Initiative Research Centre, University of New

South Wales, Australia <sup>4</sup>Institute of Global Environmental Change, Xi'an Jiaotong University, China

<sup>5</sup>Key Laboratory of Karst Dynamics, MLR, Institute of Karst Geology,

<sup>6</sup>Department of Earth Sciences, University of Minnesota, USA <sup>7</sup>Department of Atmospheric and Oceanic Sciences, School of Physics, Peking University, China

### Corresponding author:

Wuhui Duan, Key Laboratory of Cenozoic Geology and Environment, Institute of Geology and Geophysics, Chinese Academy of Sciences, No. 19 Beitucheng Western Road, Beijing 100029, China. Email: duanwuhui@mail.iggcas.ac.cn

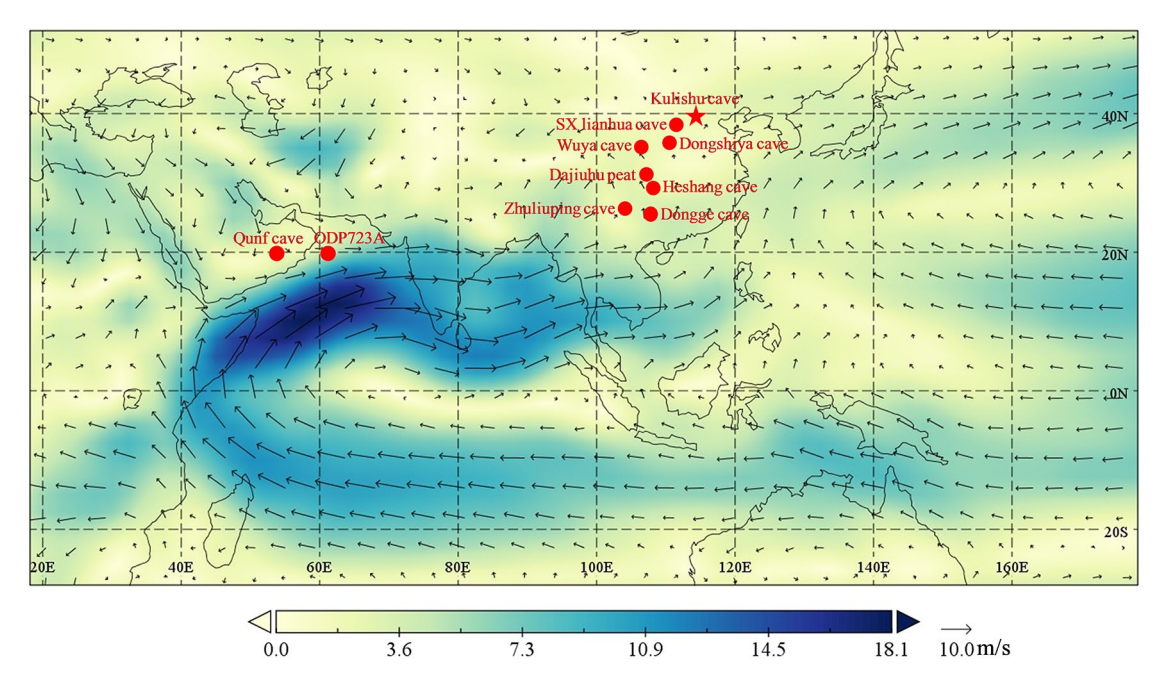


Figure 1. Map showing the locations of Kulishu Cave in this study and other Asian records mentioned. Arrows represent the average summer (June–August) vector winds at the 850 mb level from 1990 to 2020 AD based on the NCEP/NCAR reanalysis datasets (https://www.esrl.noaa.gov/psd/cgi-bin/data/composites/printpage.pl).

and more evidence should be collected to clarify the geographical extent of these smaller climate anomalies.

In the East Asian summer monsoon (EASM) region of China, lake sediment, speleothem, and peat records have also shown a series of abrupt collapses of the monsoon during the early Holocene (Cai et al., 2008; Yang et al., 2019; Zhang et al., 2018a). Excluding those occurring at around 8.2 and 9.2/9.3 ka BP, however, other short-lived monsoon anomalies lack sufficient evidence; specifically, their timing, structure, and geographical extent are not well documented. Even for the best-studied 8.2 and 9.2/9.3 ka events, remarkable differences are observed between north and south Chinese records. The 9.2/9.3 ka event is the most significant climate anomaly during the early Holocene in south Chinese peat and stalagmite records (Dykoski et al., 2005; Zhang et al., 2018b), while it is very inconspicuous in north Chinese records (Dong et al., 2018; Tan et al., 2020; Yang et al., 2019). The site-specific characteristics of different records may be responsible for this discrepancy, but the possibility of distinct climate sensitivity to high- and low-latitude forcing between north and south China should not be neglected (Zhang et al., 2018b).

In this work, a new decadal-scale stalagmite  $\delta^{18}O$  record (KLS12) covering 10.4–6.5 ka BP from Kulishu cave in Beijing, north China was combined with the previous published stalagmite  $\delta^{18}O$  record (BW-1) covering 10.4–14.0 ka BP in the same cave (Ma et al., 2012) to report the timing and detailed structure of early Holocene climate anomalies. The Kulishu cave is close to the northern limit of the EASM (Xiao et al., 2008), where precipitation is very sensitive to fluctuations of the EASM, and even small changes in moisture trajectories and/or temperature could probably have a remarkable imprint on precipitation  $\delta^{18}O$ . Thus, Kulishu stalagmite  $\delta^{18}O$  records allow us to clarify the characteristics of short-lived climate oscillations during the early Holocene.

### Materials and methods

### Cave site and stalagmite sample

Stalagmite KLS12 was collected from Kulishu Cave (39°41′N, 115°39′E, altitude 610 m above sea level) in Beijing, north China, near the northern limit of the EASM (Duan et al., 2014; Ma et al., 2012; Xiao et al., 2008) (Figure 1). The cave developed at a depth



Figure 2. Polished slab of stalagmite KLS12.

of nearly 60 m below the surface in the Middle Proterozoic dolomite; full regional and local climate and cave descriptions can be found in Duan et al. (2014) and Ma et al. (2012).

Found 100 m from the cave entrance, KLS12 is 16 cm high and 13.5 cm wide with a candlestick shape, and the growth axis changes at a depth of 5.5 cm (Figure 2). This stalagmite is composed of compact white calcite without any visible post-depositional recrystallization (Figure 2). The stalagmite BW-1 was described by Ma et al. (2012).

### Methods

Ten sub-samples (approximately 200 mg) were drilled along the stalagmite growth axis for <sup>230</sup>Th dating. Then, the powdered subsamples were completely dissolved and spiked with mixed

<sup>229</sup>Th-<sup>233</sup>U-<sup>236</sup>U. Uranium and thorium fractions were separated on 2 ml anion exchange columns following the standard techniques (Edwards et al., 1987). The separated uranium and thorium solutions were measured using a multi-collector inductively coupled plasma mass spectrometer (MC-ICP-MS) (Thermo Fisher Scientific Neptune/Plus). Of the ten subsamples, two (at depths of 97 and 117 cm) were analyzed at the Uranium-series Dating Laboratory, Institute of Geology and Geophysics, Chinese Academy of Sciences using MC-ICP-MS (Neptune plus), and the others were analyzed at the Minnesota Isotope Laboratory, Department of Earth Sciences, University of Minnesota using MC-ICP-MS (Neptune). These procedures are similar to those described by Cheng et al. (2013).

A total of 351 sub-samples (typically 50 µg) for stable isotopic composition (oxygen and carbon) measurements were collected via two methods: (1) drilled using a 0.3 mm carbide dental burr at an average interval of 0.5 mm through the whole profile and (2) shaved using a knife at an average resolution of approximately 10 sub-samples per mm at the depth of 43.5-56 mm. Powdered subsamples were analyzed on a Finnigan MAT-253 mass spectrometer equipped with a Kiel Carbonate Device IV at the Environmental Isotope Laboratory, Institute of Geology and Geophysics, Chinese

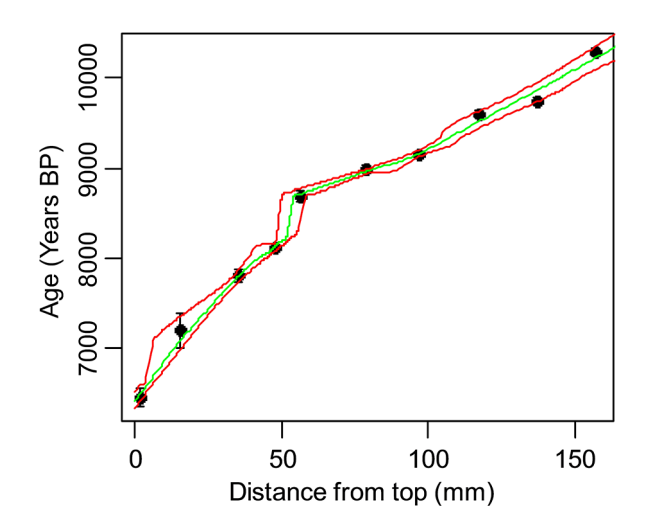


Figure 3. Age-depth plot for stalagmite KLS12. The <sup>230</sup>Th age model was established using the StalAge algorithm (Scholz and Hoffmann, 2011). The green line indicates the derived age model, and the red lines represent the 95% uncertainty envelopes. Error bars indicate 20 uncertainties.

Academy of Sciences. All oxygen isotope values are reported as δ<sup>18</sup>O (‰) relative to the Vienna Pee Dee Belemnite (VPDB) standard. An international standard NBS-19 was run for every six samples to confirm the error within 0.1% (1 $\sigma$ ). Based on <sup>230</sup>Th dating results, the temporal resolution of oxygen isotope data ranges between ~1 and 38 years, averaging 11 years.

To objectively identify the climatic anomaly superimposed on the background, the CLIM-X-DETECT algorithm (Mudelsee, 2006), a robust time-dependent extreme detection method, was applied to examine the time series. The CLIM-X-DETECT algorithm estimates the time-dependent trend and variability robustly by running median (MED) and running median of absolute distances to the median (MAD), respectively. The one standard deviation band was calculated by running MED ±1.48\*running MAD (a normal distribution has a standard deviation equal to 1.48\*MAD), which is used to define the extreme detection threshold. The unevenly spaced record was linearly interpolated to create a 10-year resolution time series, similar to the NGRIP  $\delta^{18}$ O record. The running bandwidth is set as 750 years for each record, which is longer than the typical duration of the centennial-scale anomalies and short enough for the smoothed curve to capture the gradual trend.

## Results

## Chronology

 $^{230}\text{Th}$  dates of KLS12 range from 10.3  $\pm$  0.04 ka BP at 2 mm from top to  $6.46 \pm 0.10$  ka BP at a depth of 157 mm. All dates are in stratigraphic order within the errors (2 $\sigma$ ), ranging from 32 to 196 years. The chronology was based on a polynomial fit to the age-depth curve of the <sup>230</sup>Th data using the StalAge Monte-Carlo simulation, and the 95% confidence limit was calculated from the distribution of simulated fits (Figure 3; Table 1) (Scholz and Hoffmann, 2011).

## δ<sup>18</sup>O profile

The KLS12  $\delta^{18}$ O varies between -10.13% and -8.06%, with an average of -9.08% (Figure 4). There is a ~20-year contemporaneous growth interval at around 10.4ka BP between KLS12 and the published BW-1 data (Ma et al., 2012). Because the BW-1  $\delta^{18}$ O is ~0.3% lower than KLS12  $\delta^{18}$ O at the coeval interval, the δ<sup>18</sup>O data of BW-1 was plus 0.3‰ to remove this small system deviation and then composited with that of KLS12 (Figure 4). Here, we select the interval from 11.5 to 6.4ka BP of the

**Table 1.**  $^{230}$ Th dating results for stalagmite KLS12. The errors are  $2\sigma$  uncertainties.

Depth (mm)	Sample number	<sup>238</sup> U (ppb)	<sup>232</sup> Th (ppt)	$^{230}$ Th/ $^{232}$ Th (atom-ic $\times$ 10 <sup>-6</sup> )	$\delta^{234}$ U* (measured)	<sup>230</sup> Th/ <sup>238</sup> U (activity)	<sup>230</sup> Th Age (year) (un- corrected)	<sup>230</sup> Th Age (year) (cor- rected)	$\delta^{234}$ U <sub>Initial</sub> ** (corrected)	<sup>230</sup> Th Age (year BP)*** (corrected)
2	KLS-12-1	183.7 ± 0.2	1242 ± 25	215 ± 4	485.8 ± 1.7	0.0883 ± 0.0004	6656 ± 29	6524 ± 98	495 ± 2	6462 ± 98
15.5	KLS-12-2	$\textbf{181.3} \pm \textbf{0.2}$	$2467 \pm 49$	$119 \pm 2$	$\textbf{465.8} \pm \textbf{2.4}$	$0.0982 \pm 0.0006$	$\textbf{7533} \pm \textbf{46}$	$\textbf{7265} \pm \textbf{196}$	$475\pm2$	$\textbf{7203} \pm \textbf{196}$
35.5	KLS-12-4	$\textbf{232.2} \pm \textbf{0.3}$	$\textbf{813} \pm \textbf{16}$	$\textbf{477} \pm \textbf{10}$	439.1 $\pm$ 2.3	$0.1014 \pm 0.0005$	$7941 \pm 45$	$7871\pm67$	$449\pm2$	$\textbf{7809} \pm \textbf{67}$
48	KLS-12-5	$308.1\pm0.3$	$547\pm11$	$983 \pm 20$	$451.5\pm1.7$	$0.1058 \pm 0.0005$	$\textbf{8220} \pm \textbf{40}$	$\textbf{8185} \pm \textbf{47}$	$\textbf{462} \pm \textbf{2}$	$\textbf{8123} \pm \textbf{47}$
56.5	KLS-12-6	$283.3 \pm 0.3$	$837 \pm 17$	$\textbf{618} \pm \textbf{13}$	423.1 $\pm$ 2.2	$0.1108 \pm 0.0005$	$8802 \pm 44$	$8742 \pm 61$	$434\pm2$	$8680 \pm 61$
78.5	KLS-12-7	$\textbf{506.0} \pm \textbf{1.0}$	$712\pm14$	$1328\pm27$	$\textbf{417.6} \pm \textbf{2.1}$	$0.1133 \pm 0.0003$	$\textbf{9050} \pm \textbf{30}$	$9021\pm36$	$\textbf{428} \pm \textbf{2}$	$\textbf{9002} \pm \textbf{36}$
97	KLS-12-8	$\textbf{508.0} \pm \textbf{1.0}$	$465 \pm 9$	$2075 \pm 42$	$419.1\pm2.0$	$0.1151 \pm 0.0003$	$\textbf{9187} \pm \textbf{29}$	$\textbf{9168} \pm \textbf{32}$	$430\pm2$	$\textbf{9149} \pm \textbf{32}$
117	KLS-12-9	$\textbf{523.5} \pm \textbf{0.7}$	$\textbf{392} \pm \textbf{8}$	$2662 \pm 55$	$416.1 \pm 2.1$	$0.1208 \pm 0.0004$	$9686 \pm 37$	9671 $\pm$ 38	$\textbf{428} \pm \textbf{2}$	$9609 \pm 38$
137	KLS-12-10	$507.1\pm0.8$	$628\pm13$	$1625\pm33$	$408.3 \pm 2.3$	$0.1220 \pm 0.0004$	$\textbf{9838} \pm \textbf{38}$	$\textbf{9813} \pm \textbf{42}$	$\textbf{420} \pm \textbf{2}$	975 I $\pm$ 42
157	KLS-12-11	$556.6 \pm 0.6$	$349\pm7$	$3342\pm69$	$396.7 \pm 1.7$	$0.1272 \pm 0.0004$	$\textbf{10,370} \pm \textbf{34}$	$\textbf{10,357} \pm \textbf{35}$	$408\pm2$	$\textbf{10,295} \pm \textbf{35}$

<sup>\*</sup> $\delta^{234}$ U = ([ $^{234}$ U/ $^{238}$ U]<sub>activity</sub>-I) × I000.

\*\* $\delta^{234}$ U<sub>initial</sub> was calculated based on <sup>230</sup>Th age (T), that is,  $\delta^{234}$ U<sub>initial</sub> =  $\delta^{234}$ U<sub>measured</sub> ×  $\epsilon \lambda^{234}$ ×<sup>T</sup>.

Corrected <sup>230</sup>Th ages assume the initial <sup>230</sup>Th/<sup>232</sup>Th atomic ratio of  $4.4 \pm 2.2 \times 10^{-6}$ . Those are the values for a material at secular equilibrium, with the bulk earth  $^{232}\text{Th}/^{238}\text{U}$  value of 3.8.The errors are arbitrarily assumed to be 50%.

<sup>\*\*</sup>B.P. stands for "Before Present" where the "Present" is defined as the year 1950 AD.

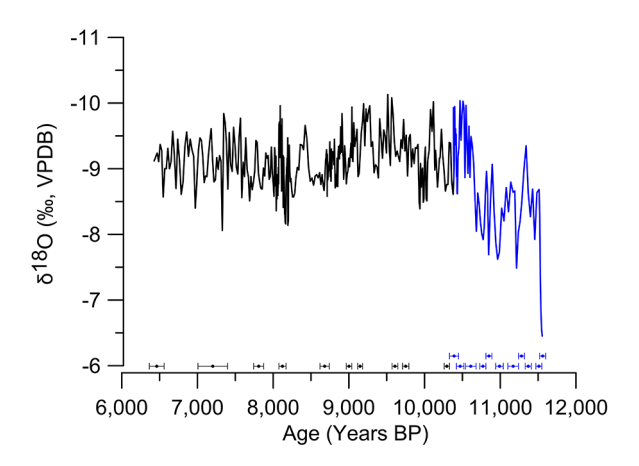


**Figure 4.**  $\delta^{18}$ O profiles of stalagmite KLS12 (black) and BW-1 (blue). The  $\delta^{18}$ O data of BW-1 (Ma et al., 2012) is plus 0.3% to remove the small system deviation. <sup>230</sup>Th dating errors (2 $\sigma$ ) are indicated at the bottom.

composite KLS record to clarify the early Holocene climate anomalies (Figure 4).

## **Discussion**

# Interpretation of $\delta^{18}$ O profile

The speleothem  $\delta^{18}$ O was mainly controlled by the recharging drip water  $\delta^{18}O$  and/or cave temperature. The temperature-dependent fractionation between calcite and water is -0.23%/°C (Friedman and O'Neil, 1977), and the range of temperature fluctuation during the early Holocene to mid-Holocene was within 1°C (Zhao et al., 2019), therefore, the amplitude of this record (1.88‰) must result largely from variations in drip water  $\delta^{18}$ O rather than the cave temperature. In turn, drip water  $\delta^{18}\mbox{O}$  in north China, in most cases, is close to the weighted average oxygen isotope composition of local meteoric precipitation (Duan et al., 2016). Additionally, the significant coherence between KLS and other cave  $\delta^{18}O$  records in north China further confirms the reliability of our record as a regional precipitation  $\delta^{18}$ O signal. Thus, following a previous study (Liu et al., 2014), we presuppose that the KLS  $\delta^{18}$ O is a proxy of EASM intensity, with depleted  $^{18}$ O indicating stronger southerly winds.

# Early Holocene climate anomalies in KLS $\delta^{18}O$ record

Based on the CLIM-X-DETECT algorithm (Mudelsee, 2006), five centennial-scale weak summer monsoon episodes (positive deviation from  $\sigma$  variation band) were identified and denoted as WM1-WM5, centered at approximately 11.5, 11.0, 10.0, 9.4, and 8.2 ka BP (Figure 5b). Among them, WM1, WM4, and WM5 are correlated with the well-known PBO, 9.2/9.3, and 8.2 ka events, respectively, all of which have been widely identified in various archives worldwide (Figure 5) (Alley et al., 1997; Cai et al., 2008; Came et al., 2007; Cheng et al., 2009; Fleitmann et al., 2008; Rasmussen et al., 2007; Zhang et al., 2018a). WM2 and WM3 can also be correlated within errors with the cold climate anomalies in the NGRIP, lacustrine, tree-ring, speleothem, and marine records in the Northern Hemisphere (Figure 5) (Björck et al., 2001; Boch et al., 2009; Cai et al., 2008; Hou et al., 2012; Rasmussen et al., 2007). Additionally, there are one or two data points exceeding the extreme detection threshold between 7.4 and 7.0 ka BP, which are possibly corresponding to the 7.2 ka climate event identified in some stalagmite records (Feng et al., 2020; Zhang et al., 2021). Given that the resolution of our record is not high enough to verify this monsoon collapse, here, we mainly focus on the more remarkable climate anomalies during early Holocene.

## The 8.2 ka climate anomaly

The isotopic maximum of the 8.2 ka climate anomaly occurred at 8.20 ka BP in our record, with high  $\delta^{18}$ O values deviation from the  $\sigma$  variation band between 8.32 and 8.12 ka BP (Figure 6a). The timing and duration are in excellent agreement with other well-dated records worldwide (Figure 5) (Alley et al., 1997; Came et al., 2007; Cheng et al., 2009; Rasmussen et al., 2007). Our record reveals a separate, earlier  $\delta^{18}$ O-enrichment excursion occurring between 8.74 and 8.47 ka BP, centered at 8.60 ka BP (Figure 6a). This weak monsoon episode has also been observed in other speleothem  $\delta^{18}O$  records in the Asian summer monsoon region (Dong et al., 2018; Fleitmann et al., 2003; Liu et al., 2013; Tan et al., 2020), which is broadly coeval with a prominent multi-centennial cooling preceding the 8.2 ka event identified in terrestrial and marine archives from the wider circum-North-Atlantic region (Ellison et al., 2006; Rohling and Pälike, 2005) as well as an enhanced dust supply to Greenland over this interval inferred from the GISP2 potassium record (O'Brien et al., 1995). The model data suggested a two-step pattern for the final drainage of Lakes Agassiz-Ojibway in separate 3.6 and 1.6 Sv pulses (for a period of 1 year) (Figure 7a), possibly accounting for the two-step structure of 8.2 ka event (Clarke et al., 2004; Teller and Leverington, 2004). Alternatively, three smaller outbursts of Lakes Agassiz-Ojibway occurring between 8.9 and 8.5 ka BP (Figure 7a) and/or the freshwater release from Hudson Bay Ice Saddle collapse around 8.6ka BP may be responsible for the climate anomaly proceeding the 8.2 ka event (Gauthier et al., 2020). Similarly, the two-step structure was also observed for some climate anomalies during mid and late-Holocene, such as 7.2, 5.5, and 2.8 ka events, which was suggested to be caused by the declined solar activity, whose impact was possibly amplified by the coeval freshwater discharge and/or shift of Inter-tropical Convergence Zone (ITCZ) (Feng et al., 2020; Tan et al., 2020). Following this hypothesis, a small decrease of irradiance occurring around 8.2 ka BP, derived from the atmospheric  $\Delta^{14}$ C record (Stuiver et al., 1998), was also one candidate for the trigger of the 8.2 ka event.

## The 9.2/9.3 ka climate anomaly

The KLS  $\delta^{18}O$  record shows a clear abrupt positive deviation (~1.0‰) from 9.41 to 9.31 ka BP, centered at 9.36 ka BP (Figure 6b), which corresponds to the 9.2/9.3 ka event in the NGRIP δ<sup>18</sup>O record (Figures 5a and 7b) as well as other stalagmite, tree ring, lacustrine, peat, and marine sediment records within the age uncertainties (Figure 5) (Dykoski et al., 2005; Fleitmann et al., 2008; Rasmussen et al., 2007; Zhang et al., 2018b). Compared to the 8.2 ka event, the signal of 9.2 ka event in our record is much weaker, with shorter duration and smaller amplitude (Figure 5b) consistent with SX Lianhua cave (Figure 5c), Wuya cave, and Dongshiya cave records in north China (Dong et al., 2018; Tan et al., 2020; Zhang et al., 2018a); however, this signal differs from the Dongge cave record (Figure 5d) and the peat sediment record of Dajiuhu basin in south China (Dykoski et al., 2005; Zhang et al., 2018b), the Qunf cave record in Oman (Figure 5e) (Fleitmann et al., 2008), as well as the marine sediment record from the Arabian Sea (Gupta et al., 2003). For most records in northern high latitude regions, the signal of the 9.2 ka event, with a shorter duration and less/similar amplitude of drop in temperature, is less significant compared to the 8.2 ka event (Boch et al., 2009; Porinchu et al., 2019; Rasmussen et al., 2007), albeit with a few exceptions, such as Arolik lake and Ammersee lake records (Grafenstein et al., 1999; Hu et al.,

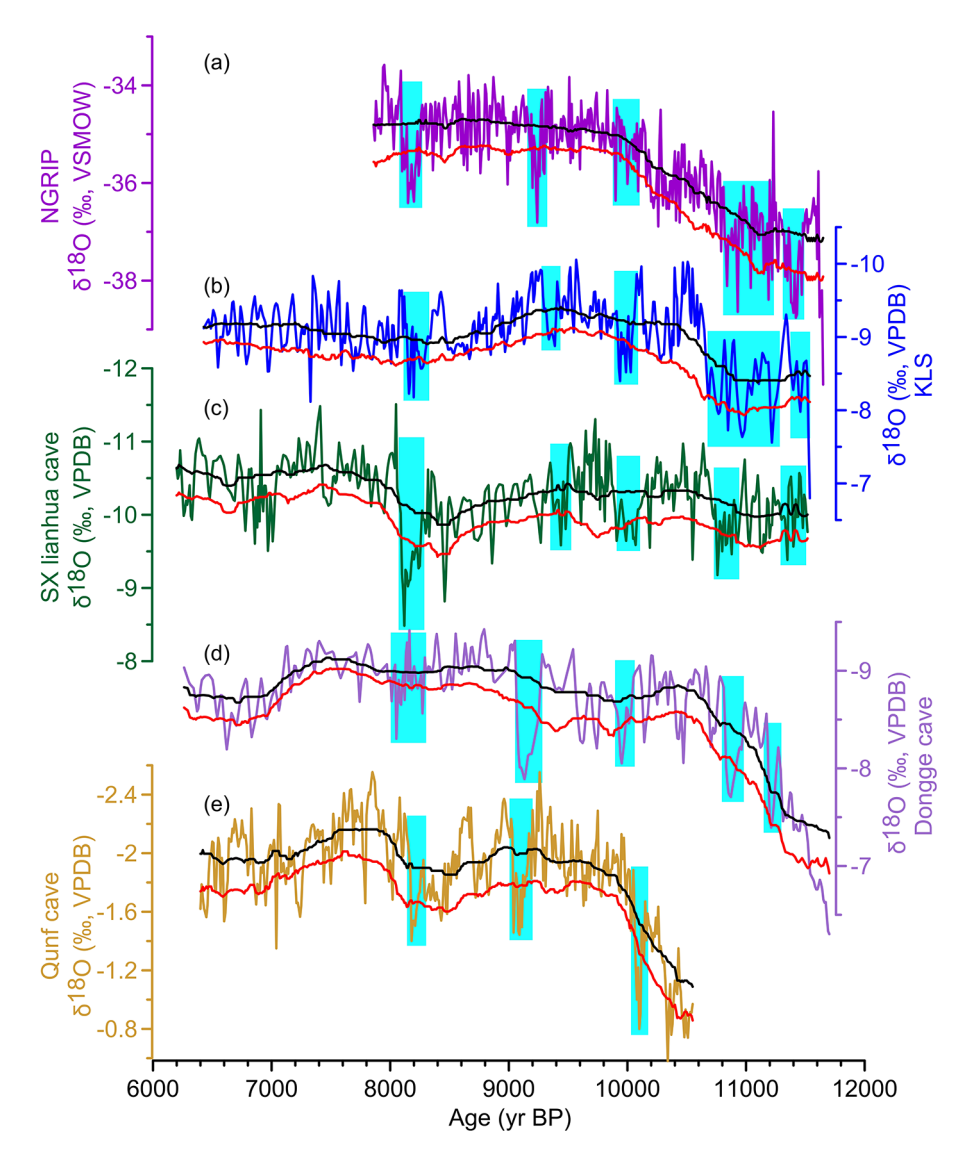


**Figure 5.** Comparison of KLS  $\delta^{18}$ O record with Greenland ice core  $\delta^{18}$ O and other speleothem  $\delta^{18}$ O records from Asian summer monsoon region. (a) NGRIP  $\delta^{18}$ O record (Rasmussen et al., 2007). Speleothem  $\delta^{18}$ O profiles from (b) Kulishu (this study and Ma et al., 2012), (c) SX Lianhua (Dong et al., 2018), (d) Dongge (Dykoski et al., 2005), and (e) Qunf caves (Fleitmann et al., 2008). Black and red lines denote the 750-year running medians and one standard deviation bands, respectively, which are calculated by the CLIM-X-DETECT algorithm (Mudelsee, 2006). Cyan bars mark the early Holocene climate anomalies defined by exceeding one standard deviation band (red line) of each profile.

2003). Most previous studies suggested freshwater outburst into the North Atlantic as a trigger for the 9.2/9.3 ka event (Figure 7a), similar to the 8.2 ka event. However, the more significant signal of the 9.2/9.3 ka event in most low latitudes relative to most mid-high latitudes cannot be well explained solely by freshwater forcing. This discrepancy may be accounted for by the site-specific characteristics of different records. Alternatively, an attenuation of irradiance around 9.45 ka BP is a candidate for the trigger (Zhang et al., 2018b).

Additionally, our record shows a separate, later  $\delta^{18}O$ -enrichment episode ( $\sim$ 0.8‰) occurring between 9.16 and 8.95 ka BP (Figure 5b), which is also identified in SX Lianhua and Dongshiya cave  $\delta^{18}O$  records (Figure 5c) (Cai et al., 2008; Dong et al., 2018; Zhang et al., 2018a). Similarly, there is a small-amplitude  $\delta^{18}O$ -depletion between 8.92 and 9.10 ka BP in NGRIP  $\delta^{18}O$  record (Figures 5a and 7b) (Rasmussen et al., 2007). This smaller climate anomaly after the 9.2/9.3 ka event appears to be related to a  $\sim$ 0.3 Sv (for a period of 1 year) freshwater outburst from Lakes Agassiz-Ojibway occurring at 9.17 ka BP (Figure 7a) (Teller and Leverington, 2004). Nevertheless, more such data are needed to fully understand this weaker climate anomaly.

### The 10.0 ka climate anomaly

The KLS δ<sup>18</sup>O record shows a markedly abrupt positive deviation (~1.5%) from 10.05 to 9.91 ka BP, centered at 9.98 ka BP, which is of comparable magnitude to the 8.2 ka event (Figure 6c). The weakened monsoon episode around 10.0 ka BP was also clearly observed in a few other speleothem  $\delta^{18}$ O records in Asian summer monsoon region, such as the SX Lianhua cave (Figure 5c), Dongshiya and Dongge caves (Figure 5d) in China, and the Qunf cave in Oman (Figure 5e) (Cai et al., 2008; Dong et al., 2018; Dykoski et al., 2005; Fleitmann et al., 2008). Additionally, speleothem, lacustrine, tree ring, Greenland ice core (Figures 5a and 7b), and marine sediment records in northern high latitudes also documented a cooling anomaly occurring around 10.0 ka BP, spanning less than 200 years (Björck et al., 2001; Boch et al., 2009; Rasmussen et al., 2007). Our record provides new convincing evidence for the 10.0 ka climate anomaly. This distinct but short climatic event likely corresponds to three smaller Lakes Agassiz-Ojibway outbursts occurring between 10.19 and 9.84 ka BP (Teller and Leverington, 2004) (Figure 7a). Alternatively, the decreased solar activity around 10.15 ka BP may be an candidate for the forcing (Björck et al., 2001).

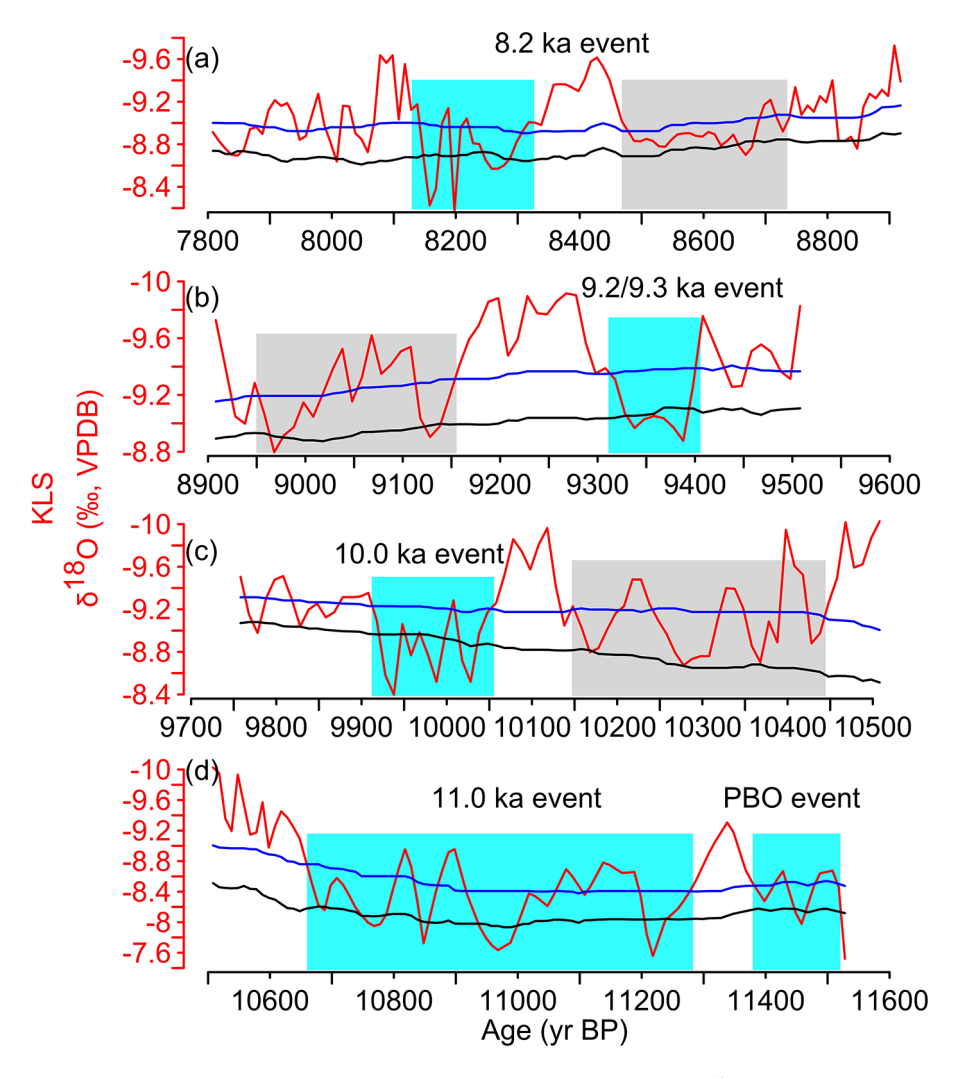


Figure 6. Structures of (a) 8.2, (b) 9.2/9.3, (c) 10.0, (d) 11.0, and PBO events identified in KLS  $\delta^{18}$ O record. Blue and black lines indicate the 750-year running medians and one standard deviation bands, respectively, which are calculated by the CLIM-X-DETECT algorithm (Mudelsee, 2006). Cyan bars mark the well-known climate events during the early Holocene. Grey bars denote the smaller climate anomalies immediately preceding or following well-known climate events.

The KLS record reveals an earlier  $\delta^{18}$ O-enrichment excursion (~1‰) occurring between 10.44 and 10.15 ka BP, centered at 10.30 ka BP (Figure 6c). A similar decreased monsoon episode around 10.30 ka BP was also identified in the SX Lianhua cave (Figure 5c), Dongshiya cave, Dongge cave (Figure 5d) as well as Qunf cave (Figure 5e) δ<sup>18</sup>O records (Cai et al., 2008; Dong et al., 2018; Dykoski et al., 2005; Fleitmann et al., 2008). Additionally, the NGRIP δ<sup>18</sup>O record (Figures 5a and 7b) and Austrian speleothem  $\delta^{18}$ O record showed a significant but short-lived cooling anomaly before the distinct 10.0 ka event, occurring around 10.30 and 10.15 ka BP, respectively (Boch et al., 2009; Rasmussen et al., 2007). Interestingly, there were also three smaller freshwater outbursts from Lakes Agassiz-Ojibway occurring between 10.60 and 10.31 ka BP (Figure 7a) (Teller and Leverington, 2004). Nevertheless, it is unclear whether the climate anomaly and Agassiz-Ojibway flood outbursts around 10.30ka BP in different records correspond with each other, and more highly resolved and precisely dated records are required to clarify the spatial distribution and underlying dynamic mechanisms.

## PBO and 11.0 ka events

The KLS  $\delta^{18}$ O record shows a positive deviation ( $\sim$ 1.2%) immediately after the end of the Younger Dryas, spanning from 11.51 to 11.38 ka BP (Figure 6d), which possibly correlates with the well-known PBO event documented in detail in European terrestrial

records and Greenland ice core δ<sup>18</sup>O records (Figures 5a and 7b) (Björck et al., 1996; Goslar et al., 1993; Rasmussen et al., 2007). The PBO event was also identified in a few other Chinese speleothem  $\delta^{18}O$  records, although there is a ~100-year age offset between north and south China. For example, in Dongshya and SX Lianhua cave records in north China, it occurred around 11.30 ka BP (Figure 5c) (Cai et al., 2008; Dong et al., 2018), which is consistent with our record, while in Dongge (Figure 5d) and Zhuliuping cave records in south China it occurred around 11.20ka BP (Dykoski et al., 2005; Huang et al., 2016). Additionally, the signal of the PBO event in all the speleothem records in China is less significant than that in Greenland and European records, possibly suggesting that it is a high-latitude-forcing climate anomaly. Meanwhile, the slightly shorter duration of the PBO event in south Chinese cave records compared to that in north Chinese cave records, provides one more evidence for the possibility of this high-latitude-forcing hypothesis. It is interesting to note that there was a ~0.30 Sv (for a period of 1 year) Lakes Agassiz-Ojibway outburst occurring around 11.6ka BP, ~100 years preceding the PBO event in NGRIP δ<sup>18</sup>O and our record (Figure 7), both of which are constrained by high-precision dating. Thus, our record supports the idea that the PBO climate anomaly is likely due to the Lakes Agassiz-Ojibway outburst occurring at around 11.6 ka BP (Teller and Leverington, 2004).

Additionally, our record presents a significant positive deviation (~1.5‰) immediately after the end of the PBO event, occurring between 11.29 and 10.66ka BP, centered around 11.0ka BP

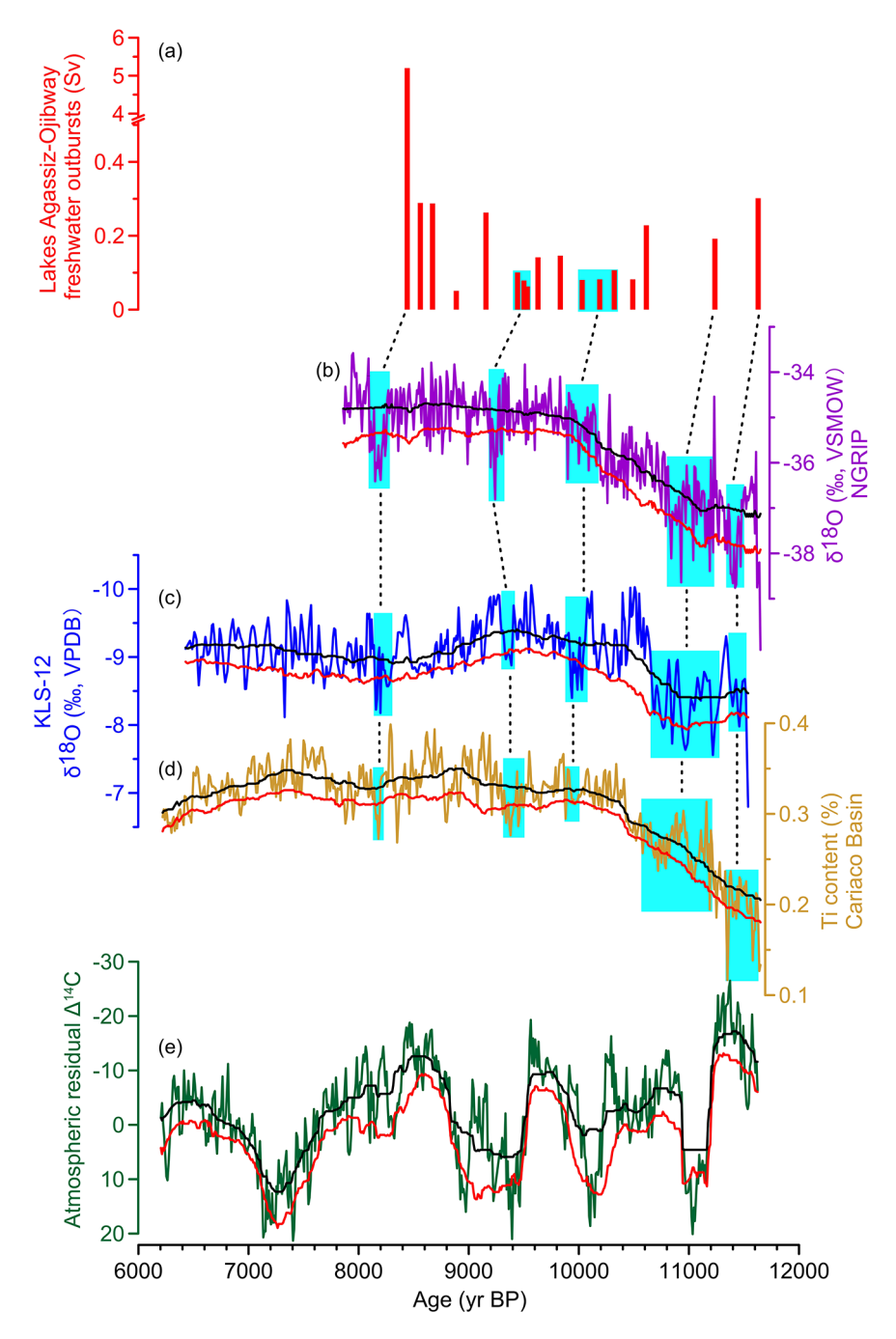


Figure 7. Comparison of KLS  $\delta^{18}$ O record with Greenland ice core  $\delta^{18}$ O and Lakes Agassiz-Ojibway freshwater outbursts records. (a) Freshwater outbursts from Lakes Agassiz-Ojibway into North Atlantic (Teller and Leverington, 2004). Each outburst has been interpreted as occurring in ~I year. (b) NGRIP  $\delta^{18}$ O record (Rasmussen et al., 2007). (c) KLS  $\delta^{18}$ O record (this study and Ma et al., 2012). (d) Ti content in the Cariaco Basin (Haug et al., 2001). (e) Atmospheric residual  $\Delta^{14}$ C (Stuiver et al., 1998). Black and red lines denote the 750-year running medians and one standard deviation bands, respectively, which are calculated by the CLIM-X-DETECT algorithm (Mudelsee, 2006). Cyan bars mark the early Holocene climate anomalies defined by exceeding one standard deviation band (red line) of each profile.

(Figure 6d). This decreased monsoon episode was also identified in speleothem  $\delta^{18}O$  records from the SX Lianhua cave (Figure 5c) and Dongshiya cave in north China and Dongge cave (Figure 5d) in south China (Cai et al., 2008; Dong et al., 2018; Dykoski et al., 2005), albeit for different durations. It is probably corresponding to a centennial-scale cooling anomaly occurring between 11.21 and 10.80 ka BP in NGRIP  $\delta^{18}O$  record (Figures 5a and 7b) (Rasmussen et al., 2007). Interestingly, there was a smaller freshwater outburst from Lakes Agassiz-Ojibway occurring around 11.2 ka BP (Figure 7a), which may be a trigger for the 11.30 ka climate anomaly (Teller and Leverington, 2004). Nevertheless, the correlation is very tenuous because of the distinct lack of high-precision and high-resolution records.

### Dynamic mechanisms

As mentioned above, all five significant and three smaller centennial-scale monsoon collapses during the early Holocene in our record correspond to the cooling anomalies identified in northern high latitudes, all of which are linked to one or more freshwater outbursts from Lakes Agassiz-Ojibway (Teller and Leverington, 2004) (Figure 7). Thus, our data support the hypothesis of freshwater forcing of rapid climate anomalies during the early Holocene (Cheng et al., 2009; Clark et al., 2002; Jennings et al., 2015; Porinchu et al., 2019; Teller and Leverington, 2004; Young et al., 2011; Yu et al., 2010). Freshwater outbursts to the North Atlantic Ocean would slow down the Atlantic Meridional Overturning Circulation (AMOC) and reduce the surface ocean heat transport

to the North Atlantic region (Broecker, 1994). In turn, cooling in the high northern latitude region would push the ITCZ southward and weaken the EASM (Zhang and Delworth, 2005). The general southward shift of the ITCZ during these weak monsoon events derived from the decrease of the Ti content in the Cariaco Basin (Figure 7d) supports this view.

Nevertheless, freshwater forcing alone would not well explain the more remarkable signal of 9.2/9.3 ka event in most low-latitude records (Figure 5) compared to that in most midhigh-latitude records (Zhang et al., 2018b). A remarkable minimum solar output around 9.45 ka BP is a potential driving force that may directly affect low-latitude climate (Figure 7e). On the one hand, the attenuation of irradiance would reduce the thermal contrast between the continent and ocean, in turn, weaken EASM intensity (Zhang et al., 2018b). On the other hand, it would induce a comparatively warmer average condition in the eastern equatorial Pacific (El Nino-like condition) (Emile-Geay et al., 2007; Marchitto et al., 2010), which is normally associated with weakened EASM intensity (Kumar et al., 2006; Parthasarathy et al., 1994; Tan, 2014). To this extent, we suggest that the 9.2/9.3 ka climate anomaly was a result of the co-influence of freshwater outburst and decreased solar activity. As mentioned above, the irradiance was also decreased during the 8.2 ka event, but its decreasing amplitude is much smaller than that around 9.2/9.3 ka event (Figure 7e), which is possibly accounted for the different spatial pattern of these two climate anomalies.

### **Conclusions**

Five remarkable centennial-scale weak summer monsoon episodes were identified around 11.5, 11.0, 10.0, 9.4, and 8.2 ka BP in the KLS  $\delta^{18}$ O record in north China. Moreover, three smaller monsoon collapses were observed around 8.60, 9.0, and 10.3 ka BP. The 8.2 ka event is marked by two distinct monsoon collapses centered around 8.60 and  $8.20\,\mathrm{ka}$  BP. The  $9.2/9.3\,\mathrm{ka}$ event in our record occurred around 9.4 ka BP, of which the duration and amplitude are not as significant as those in south Chinese cave records. All weak summer monsoon excursions are coeval with cooling anomalies in northern high-latitude records as well as freshwater outbursts from Lakes Agassiz-Ojibway within dating errors. Thus, our data support the idea that rapid climate anomalies during the early Holocene were mainly provoked by freshwater delivery to the North Atlantic Ocean. In particular, the co-influence of decreased solar activity and freshwater outburst is the most likely factor inducing the 9.2/9.3 ka event.

### Acknowledgements

We are grateful to Professor Andy Baker for his helpful comments. We thank Dr. Xu Wang and Linlin Cui for the help with the stable isotope analysis.

### **Funding**

The author(s) disclosed receipt of the following financial support for the research, authorship, and/or publication of this article: This research was supported by the National Key Research and Development Program of China (2017YFA0603401), the Strategic Priority Research Program of Chinese Academy of Sciences (Grant No. XDB26020000), National Natural Science Foundation of China (Grant Nox. 41772184, 41731174, 41472150 and 41888101), and U.S. NSF (1702816). The datasets will be uploaded to https://www.ncdc.noaa.gov/data-access/paleoclimatology-data/datasets/speleothem

### **ORCID iD**

Wuhui Duan https://orcid.org/0000-0003-3078-040X

#### References

- Alley RB, Mayewski PA, Sowers T et al. (1997) Holocene climatic instability: A prominent, widespread event 8200 yr ago. *Geology* 25(6): 483–486.
- Björck S, Kromer B, Johnsen S et al. (1996) Synchronized terrestrialatmospheric deglacial records around the North Atlantic. *Science* 274(5290): 1155–1160.
- Björck S, Muscheler R, Kromer B et al. (2001) High-resolution analyses of an early Holocene climate event may imply decreased solar forcing as an important climate trigger. *Geology* 29(12): 1107–1110.
- Boch R, Spötl C and Kramers J (2009) High-resolution isotope records of early Holocene rapid climate change from two coeval stalagmites of Katerloch Cave, Austria. *Quaternary Science Reviews* 28(23): 2527–2538.
- Bond G, Kromer B, Beer J et al. (2001) Persistent solar influence on North Atlantic climate during the Holocene. *Science* 294(5549): 2130–2136.
- Broecker WS (1994) Massive iceberg discharges as triggers for global climate change. *Nature* 372(6505): 421–424.
- Cai B, Edwards RL, Cheng H et al. (2008) A dry episode during the Younger Dryas and centennial-scale weak monsoon events during the early Holocene: A high-resolution stalagmite record from southeast of the Loess Plateau, China. Geophysical Research Letters 35(2): L02705.
- Came RE, Oppo DW and McManus JF (2007) Amplitude and timing of temperature and salinity variability in the subpolar North Atlantic over the past 10 k.y. *Geology* 35(4): 315–318.
- Cheng H, Fleitmann D, Edwards RL et al. (2009) Timing and structure of the 8.2 kyr B.P. event inferred from δ18O records of stalagmites from China, Oman, and Brazil. *Geology* 37(11): 1007–1010.
- Cheng H, Lawrence Edwards R, Shen C-C et al. (2013) Improvements in <sup>230</sup>Th dating, <sup>230</sup>Th and <sup>234</sup>U half-life values, and U-Th isotopic measurements by multi-collector inductively coupled plasma mass spectrometry. *Earth and Planetary Science Letters* 371–372: 82–91.
- Clark PU, Pisias NG, Stocker TF et al. (2002) The role of the thermohaline circulation in abrupt climate change. *Nature* 415(6874): 863–869.
- Clarke GKC, Leverington DW, Teller JT et al. (2004) Paleohydraulics of the last outburst flood from glacial Lake Agassiz and the 8200 BP cold event. *Quaternary Science Reviews* 23(3–4): 389–407.
- Dong J, Shen C-C, Kong X et al. (2018) Rapid retreat of the East Asian summer monsoon in the middle Holocene and a millennial weak monsoon interval at 9 ka in northern China. *Journal of Asian Earth Sciences* 151: 31–39.
- Duan W, Ruan J, Luo W et al. (2016) The transfer of seasonal isotopic variability between precipitation and drip water at eight caves in the monsoon regions of China. *Geochimica Et Cosmochimica Acta* 183: 250–266.
- Duan W, Tan M, Ma Z et al. (2014) The palaeoenvironmental significance of δ13C of stalagmite BW-1 from Beijing, China during Younger Dryas intervals inferred from the grey level profile. *Boreas* 43(1): 243–250.
- Dykoski CA, Edwards RL, Cheng H et al. (2005) A high-resolution, absolute-dated Holocene and deglacial Asian monsoon record from Dongge Cave, China. *Earth and Planetary Science Letters* 233(1–2): 71–86.
- Edwards RL, Chen JH and Wasserburg GJ (1987) <sup>238</sup>U-<sup>234</sup>U-<sup>230</sup>Th systematics and the precise measurement of time over the past 500,000 years. *Earth and Planetary Science Letters* 81(2–3): 175–192.
- Ellison CRW, Chapman MR and Hall IR (2006) Surface and deep ocean interactions during the cold climate event 8200 years ago. *Science* 312(5782): 1929–1932.

Emile-Geay J, Cane M, Seager R et al. (2007) El Niño as a mediator of the solar influence on climate. *Paleoceanography* 22(3): PA3210.

- Feng X, Yang Y, Cheng H et al. (2020) The 7.2 ka climate event: Evidence from high-resolution stable isotopes and trace element records of stalagmite in Shuiming Cave, Chongqing, China. *The Holocene* 30: 145–154.
- Fleitmann D, Burns SJ, Mudelsee M et al. (2003) Holocene forcing of the Indian monsoon recorded in a stalagmite from southern Oman. *Science* 300(5626): 1737–1739.
- Fleitmann D, Mudelsee M, Burns SJ et al. (2008) Evidence for a widespread climatic anomaly at around 9.2 ka before present. *Paleoceanography* 23(1): PA1102.
- Friedman I and O'Neil JR (1977) Compilation of stable isotope fractionation factors of geochemical interest. In: Fleischer M (ed.) Data of Geochemistry. 6th ed. Reston, VA: U.S. Geological Survey Professional Paper 440-KK.
- Gauthier MS, Kelley SE and Hodder TJ (2020) Lake Agassiz drainage bracketed Holocene Hudson Bay ice saddle collapse. *Earth and Planetary Science Letters* 544: 116372.
- Goslar T, Kuc T, Ralska-Jasiewiczowa M et al. (1993) High-resolution lacustrine record of the late glacial/Holocene transition in central Europe. *Quaternary Science Reviews* 12(5): 287–294.
- Grafenstein UV, Erlenkeuser H, Brauer A et al. (1999) A mid-European decadal isotope-climate record from 15,500 to 5000 years B.P. *Science* 284(5420): 1654–1657.
- Gupta AK, Anderson DM and Overpeck JT (2003) Abrupt changes in the Asian southwest monsoon during the Holocene and their links to the North Atlantic Ocean. *Nature* 421(6921): 354–357.
- Haug GH, Hughen KA, Sigman DM et al. (2001) Southward migration of the intertropical convergence zone through the Holocene. Science 293: 1304–1308.
- Hou J, Huang Y, Shuman BN et al. (2012) Abrupt cooling repeatedly punctuated early-Holocene climate in eastern North America. *The Holocene* 22(5): 525–529.
- Hu FS, Kaufman D, Yoneji S et al. (2003) Cyclic variation and solar forcing of Holocene climate in the Alaskan subarctic. *Science* 301(5641): 1890–1893.
- Huang W, Wang Y, Cheng H et al. (2016) Multi-scale Holocene Asian monsoon variability deduced from a twin-stalagmite record in southwestern China. *Quaternary Research* 86(1): 34–44.
- Jennings A, Andrews J, Pearce C et al. (2015) Detrital carbonate peaks on the Labrador shelf, a 13–7ka template for freshwater forcing from the Hudson Strait outlet of the Laurentide Ice Sheet into the subpolar gyre. *Quaternary Science Reviews* 107: 62–80.
- Kumar KK, Rajagopalan B, Hoerling M et al. (2006) Unraveling the mystery of Indian monsoon failure during El Niño. Science 314(5796): 115–119.
- Liu Y, Henderson GM, Hu C et al. (2013) Links between the East Asian monsoon and North Atlantic climate during the 8,200 year event. *Nature Geoscience* 6(2): 117–120.
- Liu ZY, Wen XY, Brady EC et al. (2014) Chinese cave records and the East Asia summer monsoon. *Quaternary Science Reviews* 83: 115–128.
- Ma Z, Cheng H, Tan M et al. (2012) Timing and structure of the Younger Dryas event in northern China. *Quaternary Science Reviews* 41: 83–93.
- Marchitto TM, Muscheler R, Ortiz JD et al. (2010) Dynamical response of the tropical Pacific Ocean to solar forcing during the early Holocene. *Science* 330(6009): 1378–1381.
- Mudelsee M (2006) CLIM-X-DETECT: A Fortran 90 program for robust detection of extremes against a time-dependent background in climate records. *Computers and Geosciences* 32: 141.
- O'Brien SR, Mayewski PA, Meeker LD et al. (1995) Complexity of Holocene climate as reconstructed from a Greenland ice core. *Science* 270(5244): 1962–1964.

Parthasarathy B, Munot AA and Kothawale DR (1994) All-India monthly and seasonal rainfall series: 1871–1993. *Theoretical* and Applied Climatology 49(4): 217–224.

- Porinchu DF, MacDonald GM, Moser KA et al. (2019) Evidence of abrupt climate change at 9.3 ka and 8.2 ka in the central Canadian Arctic: Connection to the North Atlantic and Atlantic Meridional overturning circulation. *Quaternary Science Reviews* 219: 204–217.
- Rasmussen SO, Vinther BM, Clausen HB et al. (2007) Early Holocene climate oscillations recorded in three Greenland ice cores. *Quaternary Science Reviews* 26(15): 1907–1914.
- Rohling E and Pälike H (2005) Centennial-scale climate cooling with a sudden cold event around 8,200 years ago. *Nature* 434: 975–979.
- Scholz D and Hoffmann DL (2011) StalAge An algorithm designed for construction of speleothem age models. *Quaternary Geochronology* 6(3–4): 369–382.
- Stuiver M, Reimer PJ, Bard E et al. (1998) INTCAL98 radiocarbon age calibration, 24,000-0 cal BP. *Radiocarbon* 40: 1041–1083.
- Tan L, Li Y, Wang X et al. (2020) Holocene monsoon change and abrupt events on the western Chinese Loess Plateau as revealed by accurately dated stalagmites. *Geophysical Research Letters* 47(21): e2020GL090273.
- Tan M (2014) Circulation effect: Response of precipitation  $\delta^{18}$ O to the ENSO cycle in monsoon regions of China. *Climate Dynamics* 42(3–4): 1067–1077.
- Teller JT and Leverington DW (2004) Glacial Lake Agassiz: A 5000 yr history of change and its relationship to the  $\delta^{18}$ O record of Greenland. *GSA Bulletin* 116(5–6): 729–742.
- Xiao J, Si B, Zhai D et al. (2008) Hydrology of Dali Lake in central-eastern Inner Mongolia and Holocene East Asian monsoon variability. *Journal of Paleolimnology* 40(1): 519–528.
- Yang X, Yang H, Wang B et al. (2019) Early-Holocene monsoon instability and climatic optimum recorded by Chinese stalagmites. *The Holocene* 29(6): 1059–1067.
- Young NE, Briner JP, Axford Y et al. (2011) Response of a marine-terminating Greenland outlet glacier to abrupt cooling 8200 and 9300 years ago. *Geophysical Research Letters* 38(24): L24701.
- Young NE, Briner JP, Rood DH et al. (2013) Age of the Fjord Stade moraines in the Disko Bugt region, western Greenland, and the 9.3 and 8.2 ka cooling events. *Quaternary Science Reviews* 60: 76–90.
- Yu S-Y, Colman SM, Lowell TV et al. (2010) Freshwater outburst from Lake Superior as a trigger for the cold event 9300 years ago. *Science* 328(5983): 1262–1266.
- Zhang N, Yang Y, Cheng H et al. (2018a) Timing and duration of the East Asian summer monsoon maximum during the Holocene based on stalagmite data from North China. *The Holocene* 28(10): 1631–1641.
- Zhang R and Delworth TL (2005) Simulated tropical response to a substantial weakening of the Atlantic thermohaline circulation. *Journal of Climate* 18(12): 1853–1860.
- Zhang W, Chang M, Yan H et al. (2021) Synchronous changes in the East Asian-Australian summer monsoons around 7.2 ka. *Palaeogeography, Palaeoclimatology, Palaeoecology* 567: 110303.
- Zhang W, Yan H, Dodson J et al. (2018b) The 9.2 ka event in Asian summer monsoon area: The strongest millennial scale collapse of the monsoon during the Holocene. *Climate Dynamics* 50(7): 2767–2782.
- Zhao L, Liu J, Liu B et al. (2019) Comparison of the summer surface air temperature and precipitation over East Asia between the Holocene Thermal Maximum and the RCP4.5 scenario. *Quaternary Sciences* 39(3): 731–741. (in Chinese)